A Peptidoglycan Amidase Mutant of Burkholderia insecticola Adapts an L-form-like Shape in the Gut Symbiotic Organ of the Bean Bug Riptortus pedestris

Shiori Goto, Tsubasa Ohbayashi, Kazutaka Takeshita, Teruo Sone, Yu Matsuura, Peter Mergaert, Yoshitomo Kikuchi

A peptidoglycan amidase mutant of *Burkholderia insecticola* adapts an L-form-like shape in the gut symbiotic organ of the bean bug *Riptortus pedestris*

Shiori Goto[1,†], Tsubasa Ohbayashi[2,3,†,*], Kazutaka Takeshita[4], Teruo Sone[5], Yu Matsuura[6], Peter Mergaert[2] and Yoshitomo Kikuchi[1,7]

Affiliations:

[1] *Graduate School of Agriculture, Hokkaido University, 060-8589 Sapporo, Japan*

[2] *Université Paris-Saclay, CEA, CNRS, Institute for Integrative Biology of the Cell (I2BC), 91198, Gif-sur-Yvette, France.*

[3] *Institute for Agro-Environmental Sciences, National Agriculture and Food Research Organization (NARO), 305-8604 Tsukuba, Japan*

[4] *Faculty of Bioresource Sciences, Akita Prefectural University, 010-0195 Akita, Japan*

[5] *Research Faculty of Agriculture, Hokkaido University, 060-8589 Sapporo, Japan*

[6] *Tropical Biosphere Research Center, University of the Ryukyus, 903-0213 Okinawa, Japan*

[7] *Bioproduction Research Institute, National Institute of Advanced Industrial Science and Technology (AIST), Hokkaido Center, 062-8517 Sapporo, Japan*

[†] equal contribution as first authors

Running headline: *Symbiont cell shape in insect gut* (33 characters)

* Corresponding author

Tsubasa Ohbayashi: E-mail, tsubasa.ohbayashi@gmail.com; Tel. and Fax., +81-29-838-8309

Abstract

Bacterial cell shape can be altered by the cell cycle, nutrient availability, environmental stress, and interaction with other organisms. The bean bug *Riptortus pedestris* possesses a symbiotic bacterium, *Burkholderia insecticola,* located in midgut crypts. This symbiont is a typical rod-shaped bacterium in *in vitro* culture conditions, whereas it alters into a spherical shape inside the gut symbiotic organ of the host insect, suggesting that host factors induce the morphological alteration of *B. insecticola*. In this study, we revealed that a deletion mutant of a peptidoglycan amidase gene (*amiC*), showing a filamentous chain-form *in vitro*, adapts a swollen L-form-like cell shape in the midgut crypts. Spatiotemporal observations of the Δ*amiC* mutant in the midgut crypts revealed that swollen cells were induced particularly prior to the molting of the insects. To clarify the underpinning mechanism of the *in vivo*-specific morphological alteration, the symbiont was cultured in 13 different conditions and its cell shape was analyzed. Swollen cells, similar to the symbiont cells in midgut crypts, were induced when the mutant was treated with fosfomycin, an inhibitor of peptidoglycan precursor biosynthesis. Taking together, these results strongly suggest that the *Burkholderia* symbiont is under control of the host insect in the midgut crypts by a cell wall-attacking agent.

(204 words < 250 words)

Key words: *Burkholderia*, gut symbiosis, cell shape, *amiC*, L-form

Introduction

Ever since Antonie van Leeuwenhoek observed in the 17th century for the first time the amazing diversity of bacteria and bacterial shapes by the use of his self-made microscope, bacterial cell morphology has attracted the attention of a broad range of microbiologists. Bacterial cell shape is intrinsically controlled by the cell wall composed of the peptidoglycan sacculus and by cytoskeleton protein complexes such as the tublin homolog FtsZ and actin-like MreB acting during cell division and cell elongation (Egan *et al*., 2020). Under particular conditions, notably when bacterial cell wall synthesis is inhibited by antibiotics or lysozyme, the cell shape can alter to a spherical form called "L-form". L-form bacteria are able to proliferate without a cell wall or with only remnants of it, and their spherical cell shape represents the energetically most stable form in adaptation to the cell turgor (Allan *et al*., 2009; Schmidtke and Carson, 1999; Strang *et al*., 1991).

Moreover, bacterial morphology is also influenced by internal factors such as the bacterial growth phase, and by external factors like nutrient availability, environmental and chemical stresses, physical constraints, predation and life inside other organisms (van Teeseling *et al*., 2017; Young, 2006). Bacteria that colonize environments inside other organisms, like endosymbionts or pathogens, sometimes adapt forms markedly deviating from their regular shape in the free-living state. A well-described example of such a cell shape alteration is found in the nitrogen-fixing legume-rhizobium symbiosis, when the rhizobial symbionts colonize the symbiotic organ, the root nodule, developed by the host plant. Rhizobia are typical rod-shaped alpha- or beta-Proteobacteria in the

free-living state in soil and *in vitro* culture conditions (Oke, 1999). The symbiotic bacteria that colonize the plant cells of the root nodule differentiate into a specialized, nitrogen-fixing form, called "bacteroid". In some legumes, bacterial cell-division is inhibited during the formation of the bacteroids but cell growth and genome replication continues, resulting in extremely enlarged bacterial cells that can be elongated, branched or spherical (Czernic *et al*., 2015; Mergart *et al*., 2006; Oke, 1999). In the root nodules, defensin-like membrane-attacking antimicrobial peptides called "Nodule-specific Cysteine Rich peptides (NCRs)" are highly expressed (Mergaert *et al*., 2003). They induce the morphological and physiological alterations in the rhizobium bacteroids (Mergaert, 2020; Mergaert, 2018).

Intracellular symbionts are also common in insects, which can carry them in specific organs called bacteriomes that are composed of symbiont-infected cells or bacteriocytes (Baumann *et al*., 2005). Bacteriocyte-associated endosymbionts are usually unable to grow in a free-living state outside of their insect host but they have free-living close relatives in the alpha-, beta-, and gamma-Proteobacteria or Bacteroidetes. These intracellular insect symbionts are often large and have morphologies very different from their rod-shaped free-living relatives. Similar to the rhizobium bacteroids in legumes, bacteriocyte symbionts can be spherical or elongated, sometimes enlarged to extreme sizes. Previous studies have shown they can have very unusual, irregular and pleomorphic shapes, forming balloon-structures with invaginations or even rosette-like forms (Bublitz *et al*., 2019; Hirota *et al*., 2017; Login *et al*., 2011; Lukasik *et al*., 2017; Okude *et al*., 2017; Shigenobu and Wilson, 2011).

Possibly, these particular differentiated bacterial forms of insect and plant endosymbionts adapt space-filling shapes to occupy optimally most volume available in their host cells.

The bean bug *Riptortus pedestris* possesses a gut symbiotic bacterium, *Burkholderia insecticola*, in a crypt-bearing posterior region of the midgut (the 4th section of the midgut, M4), where over 100 million symbiont cells are housed (Kaltenpoth and Flórez 2020; Ohbayashi *et al*., 2020; Takeshita and Kikuchi 2017). Eggs and hatchlings of *R. pedestris* are aposymbiotic (*i.e.* symbiont-free) and the insect acquires *B. insecticola* specifically from ambient soil during its development (Kikuchi *et al*. 2007; Kikuchi *et al*., 2011). Crucial in the acquisition of the symbionts is a bacteria-sorting organ of the midgut called the "constricted region", separating the anterior digestive regions of the midgut from the posterior symbiotic compartment (Ohbayashi *et al*. 2015). To pass through the constricted region and reach the crypt-bearing symbiotic gut region, the flagella motility of *B. insecticola* is pivotal (Ohbayashi *et al*. 2015) as well as other, still to be discovered molecular features (Itoh *et al*., 2019). After colonization, morphological and physiological alterations occur in *B. insecticola* (Ohbayashi *et al*., 2019): the cell shape becomes spherical, the DNA content per cell is decreased, and the lipopolysaccharide (LPS) of the cell envelope is partially altered. At the transcriptomic level, several metabolic pathways including assimilation pathways of host metabolic wastes such as sulfate and allantoin are specifically up-regulated *in vivo*, indicating that *B. insecticola* is proliferating in the bean bug midgut by recycling the host's metabolic wastes (Ohbayashi *et al*., 2019). However, it is still

110 unclear what mechanisms and molecules of the host midgut induce the morphological
111 and physiological alterations of the symbiont.
112 Bacterial N-acetylmuramyl-L-alanine amidase encoded by *amiC* is involved in
113 septal peptidoglycan cleavage during cell division (Heidrich *et al*., 2001). An *amiC*
114 (BRPE64_ACDS22630) deletion mutant of *B. insecticola* (Δ*amiC*) has a filamentous
115 form composed of chains of unseparated cells because cell division is incomplete.
116 Consequently, the mutant has lost motility and infection ability (Lee *et al*. 2015).
117 Notably, the chain-form of the Δ*amiC* mutant is nutrient-dependent: although the
118 mutant forms chains in the nutrient-rich YG (yeast extract and glucose) medium, in a
119 minimal medium the mutant forms separated cells and its motility and infection ability
120 are restored (Lee *et al*. 2015).
121 In this study, we revealed that, compared with *in vitro* conditions, a more drastic
122 morphological alteration occurs in the Δ*amiC* mutant inside the insect midgut where the
123 mutant becomes spherical and remarkably enlarged. Furthermore, to clarify the
124 underpinning mechanism of the symbiont's morphological change inside the midgut
125 crypts, we tested effects of nutrients, stress agents and antibiotics on cell morphologies
126 of the symbiont, thereby finding that the antibiotic fosfomycin could mimic the swollen
127 shape *in vitro*.
128

Materials and Methods

Insects and bacterial strains

The bean bug *R. pedestris* TKS1 inbred line is derived from a pair of wild insects collected from a soybean field in Tsukuba, Ibaraki, Japan in 2007 and has been maintained in the laboratory for over ten years. The insects were reared in a container at 25ºC under a long-day regimen (16h light-on, 8h light-off) and fed with dry soybean seeds and a cotton pad containing distilled water with 0.05% ascorbic acid. The container was replaced twice a week. For infection experiments, newborn insects were placed in a petri dish and fed as above.

A GFP-labeled *B. insecticola* wild-type strain RPE225 (Kikuchi and Fukatsu, 2014) and a GFP-labeled Δ*amiC* mutant (Lee *et al*., 2015) were used in this study. To generate a fluorescent-labeled bacterial strain, a Tn7-GFP mini-transposon was used as described previously (Kikuchi and Fukatsu, 2014). These bacteria were cultured at 27 ºC and 150 rpm agitation in YG medium [yeast extract 5.0 g/L, glucose 4.0 g/L, NaCl 1.0 g/L], or MMGlc medium (minimum medium with glucose as a sole carbon source) [$KH(PO_4)_2$ 78 mM, KH_2PO_4 122mM, $(NH_4)_2SO_4$ 7.57 mM, NaCl 3.42 mM, $MgSO_4 \cdot 7H_2O$ 0.405 µM, $FeSO_4 \cdot 7H_2O$ 8.85 µM, EDTA·2Na 11.3µM and glucose 1.0 g/L] supplemented with rifampicin 10 µg/mL and kanamycin 30 µg/mL. Bacto agar 15.0 g/L was added for solid media.

Oral administration of symbionts to the bean bug

Three days after hatching, water was removed from the plastic dish containing the newly molted 2nd instar nymphs. They were kept without water overnight. This water deprivation stimulates the next day the instant drinking of a bacterial suspension, resulting in the efficient establishment of the symbiotic infection. *B. insecticola* wild type and the Δ*amiC* mutant were pre-cultured in 3 mL MMGlu medium containing 30 µg/mL kanamycin at 27 ºC and 150 rpm in a rotary incubator; 200 µL of the overnight culture was inoculated to 3 mL MMGlu and incubated at 27 ºC and 150 rpm until the exponential growth phase. After confirmation of bacterial motility by microscopy observation, the bacterial density was adjusted to 10^7 cells/mL by measuring the optical density, and the bacterial suspension was provided to the insects as their drinking water. These insects were maintained until dissection and further analyses.

Quantitative PCR

To determine the number of *B. insecticola* symbiont cells colonizing the M4 crypts, DNA extraction was performed from the dissected M4 crypts infected with the wild type or Δ*amiC* mutant by using the QIAmp DNA Mini kit (Qiagen). A 150 base pair fragment of the *dnaA* gene was amplified by real-time quantitative PCR using KAPA SYBR Fast qPCR polymerase (KAPA Biosystems) and the primer-set BSdnaA-F (5′- AGC GCG AGA TCA GAC GGT CGT CGA T -3′) and BSdnaA-R (5′- TCC GGC AAG TCG CGC ACG CA -3′) (Kikuchi and Fukatsu, 2014). The PCR temperature profile was set to 95 ºC for 3 minutes, 40 cycles of 95 ºC for 3 seconds, 55

171 ºC for 20 seconds and 72 ºC for 15 seconds, and then 95 ºC for 5 seconds, 65 ºC for 1
172 minute and 97 ºC for 30 seconds using the LightCycler® 480 Real-Time PCR System
173 (Roche life science). The number of *B. insecticola* symbiont cells was calculated based
174 on a standard curve for the *dnaA* gene with 10, 10^2, 10^3, 10^4, 10^5, 10^6, and 10^7 copies
175 per reaction of the target PCR fragment.
176
177 ***In vitro* induction of swollen cells**
178 The *B. insecticola* wild type and Δ*amiC* mutant was pre-cultured overnight in
179 MMGlc medium, with 30 µg/mL kanamycin for the mutant, at 30 ºC and 150 rpm. The
180 overnighter was diluted with fresh MMGlc medium and incubated until the exponential
181 phase. The bacterial cells were collected by centrifugation at 15,000 rpm for 5 min at
182 room temperature. The bacterial pellet was washed with MMnoC medium (minimum
183 medium without any carbon source). Bacterial density was adjusted to OD_{600}=0.05 by
184 MMnoC medium supplemented with a carbon source: glucose 0.5%, fructose 0.5%,
185 mannitol 0.5%, yeast extract 0.3%, or maleic acid 0.2%. In the case of culture with
186 MMnoC medium without any carbon source, bacterial density was adjusted to
187 OD_{600}=0.5, and then these bacteria were incubated at 27 ºC with 150 rpm agitation. For
188 stress exposure conditions, after washing with MMGlc medium, bacterial density was
189 adjusted to OD=0.05 by MMGlc medium. Stress compounds were added as follows:
190 lysozyme from chicken egg white (c-type lysozyme; Sigma) 2.0 mg/mL, polymyxin B
191 (Sigma) 25 µg/mL, H_2O_2 125 µM, or sodium dodecyl sulfate (SDS; Sigma) 125 µM. In
192 case of fosfomycin 50 µg/mL (Sigma) exposure, bacterial density was adjusted to

193 OD_{600}=0.05 by MMMSM (minimum medium with magnesium-sucrose-maleic acid)
194 medium [$KH(PO_4)_2$ 78 mM, KH_2PO_4 122mM, $(NH_4)_2SO_4$ 7.57 mM, NaCl 3.42 mM,
195 $MgSO_4 \cdot 7H_2O$ 0.405 µM, $FeSO_4 \cdot 7H_2O$ 8.85 µM, EDTA·2Na 11.3µM, glucose 1.0
196 g/L, $MgCl_2$ 20 mM, sucrose 0.5 M and maleic acid 20 mM] modified slightly from
197 NBMSM (nutrient broth with magnesium-sucrose-maleic acid) medium (Kawai *et al.*,
198 2015). These bacteria were cultured at 27 ºC with 150 rpm agitation until middle
199 exponential phase, and then the cell shapes were investigated by epifluorescence
200 microscopy (Leica, DMI4000).

201

202 **Epifluorescence microscopy observation**

203 Insects were dissected in phosphate-buffered saline (PBS) buffer under a
204 binocular (Leica, S8APO), and the M4 crypts were collected. For observation of *in vivo*
205 bacterial cells, the M4 crypts were transferred onto a glass microscopy slide with 5 µL
206 of PBS buffer and a cover glass. Bacteria were released from the crypts by exerting a
207 pressure on the cover glass. They were observed by epifluorescence microscopy. *In*
208 *vitro* cultured bacterial cells were observed similarly.

209

210 **Confocal laser scanning microscopy observation**

For spatiotemporal observation of the M4-colonizing Δ*amiC* mutant cells, symbiotic insects at early 3rd instar stage (few hours post molting from 2nd instar), 3rd instar middle stage (1~2 days post molting from 2nd instar) and 3rd instar late stage (3~4 days post molting from 2nd instar) were dissected, and the posterior region of the midgut was collected. The tissue was stained by 3.75 µg/mL 4,6'-diamidino-2-phenylindole (DAPI), washed by PBS and then fixed by 1% paraformaldehyde, washed by PBS, mounted in 20% glycerol and observed by confocal laser scanning microscopy using a Leica TCS SP8 instrument.

Quantitative analysis of bacterial cell shape

Bacterial cells were randomly selected from microscopy pictures and their cell shape was evaluated by ImageJ software (ver.1.51) (Schneider *et al*., 2012). An individual cell was selected as Region Of Interest (ROI) and lengths of minor axis and major axis were measured. The aspect ratio as an index of circularity was calculated by dividing the minor axis length by the major axis length. Cell shape was determined by the aspect ratio shown in Supplementary Fig. S1. Parameters were measured in dividing cells and chain-forming cells. The number of investigated cells in each condition is shown in each figure (Fig. 2, Fig. 4 and Supplementary Fig. S3).

Results

The Δ*amiC* mutant of *B. insecticola* forms cell chains *in vitro* and swollen cells in the bean bug midgut

The *B. insecticola* wild-type strain was rod-shaped when cultured *in vitro* (Fig. 1A), whereas *in vivo* symbiont cells became smaller, and some of them were spherical-shaped in agreement with our previous report (Fig. 1C; Ohbayashi *et al*., 2019). In contrast, the Δ*amiC* had a strikingly different cell shape. The mutant formed long chains of unseparated cells in a nutrient-rich YG medium due to incomplete cell division as shown previously (Fig. 1B; Lee *et al*., 2015), but *in vivo* Δ*amiC* cells became spherical, and chain formation was less pronounced (Fig.1D). Strikingly, some of the spherical cells were strongly swollen (Fig. 1D).

To confirm the morphological alteration of the Δ*amiC* mutant quantitatively, image analysis of cell shape was performed by measuring the minor axis and major axis lengths of individual cells in epifluorescence microscopy pictures. The aspect ratio, calculated as the division of the minor axis length by the major axis length indicates the cellular circulation level, and the lengths of major axis and minor axis were used as a proxy to estimate bacterial cell size (Supplementary Fig. S1A). The aspect ratio varies between 0 and 1. A value close to 1 indicates a spherical cell shape, whereas strongly elongated cells have a value close to 0 (Supplementary Fig. S1B). The aspect ratio distribution of the wild type and Δ*amiC* mutant grown *in vitro* were indistinguishable and had a normal distribution with a mean aspect ratio of 0.5 (Fig. 2A-2B). However, the aspect ratio of the *in vivo* symbiont cells of both the wild type and mutant had a bi-

modal distribution, which was different from the aspect ratios of the *in vitro* grown cells (Fig. 2C-2D). The wild type symbiont cells had an aspect ratio peak at 0.6 to 0.7, slightly higher than when grown in culture and a second peak at 0.9 to 1.0. The mutant, on the other hand, had a first peak similar as the *in vitro* grown bacteria and a second major peak at 0.9 to 1.0. Notably, the proportion of spherical bacterial cells with aspect ratio larger than 0.8 was 44% for the *in vivo* Δ*amiC* mutant, whereas it was only 24% for the *in vivo* wild type (Fig. 2C-2D), showing that the alteration from rod shape to a spherical form is more pronounced in the mutant than in the wild type.

The distribution of the major and minor axis lengths of the wild type and Δ*amiC* mutant reflected the cell size reduction *in vivo* as shown previously (Fig. 2E-2H; Ohbayashi *et al*., 2019). The wild type had a mean major axis length of 2.6 µm *in vitro* and of only 1.6 µm *in vivo*, whereas the mean major axis length of the Δ*amiC* mutant was 2.3 µm *in vitro* and 1.8 µm *in vivo* (Fig. 2E-2H). Moreover, the cell size measurements revealed the presence of a small fraction of spherical *in vivo* Δ*amiC* mutant cells with axis lengths larger than 2.3 µm and up to 3.5 µm. Such very enlarged swollen cells were absent in the wild type (Fig. 2E-2H). Together, these data confirm the microscopic observation (Fig. 1D) and suggest that the *in vivo* bacterial cells had two populations with rod-shaped and spherical cells, and that majority of the Δ*amiC* mutant *in vivo* cells became spherical or swollen, some of them becoming even very large. Despite this marked difference in cell morphology, an infection test and quantification of the occupancy by the bacteria demonstrated that the Δ*amiC* mutant

was able to colonize the M4 crypts as well as the wild type in all nymph stages (Supplementary Fig. S2).

Fosfomycin can induce swollen cells *in vitro* in the *B. insecticola* Δ*amiC* mutant

Many bacteria change their cell morphology depending on the environmental conditions such as nutrient availability and bacterial stresses (van Teeseling *et al*., 2017). How are the swollen cells of the Δ*amiC* mutant produced in the midgut environment of the bean bug? To answer this question, we attempted to reproduce swollen cells *in vitro*. To this end, we investigated the cellular morphology of the wild type and the Δ*amiC* mutant, cultured in 13 different conditions. These conditions included growth in minimal medium with five different carbon sources (glucose, fructose, mannitol, yeast extract, and maleic acid) and exposure to four cell membrane stresses (fosfomycin, lysozyme, polymyxin B, and SDS), an oxidative stress (hydrogen peroxide) as well as three osmotic stresses (sucrose, glycerol, and NaCl). Out of these 13 different culture conditions, only fosfomycin exposure could induce spherical cells in the *B. insecticola* wild type, and swollen cells in the Δ*amiC* mutant (Fig. 3). Quantitative analysis (Fig. 4) demonstrated that fosfomycin exposure resulted in a distribution of the cell shape aspect ratio with one sharp peak close at 0.9 to 1.0 in the wild type and the Δ*amiC* mutant, similar to the major population of the *in vivo* Δ*amiC* mutant (Fig. 2D and Fig. 4C-4D). Moreover, in the fosfomycin-exposed Δ*amiC* mutant, 25% of the spherical cells had axis lengths of 2.3 to 3.9 μm, similar to the largest swollen *in vivo* cells of the mutant (Fig. 2H and Fig. 4H). Fosfomycin is an inhibitor of

the enzyme UDP-*N*-acetylglucosamine enolpyruvyl transferase (MurA) involved in the biosynthesis of the peptidoglycan precursor UDP-*N*-acetylglucosamine enolpyruvate (Falagas *et al*., 2016), suggesting that the swollen cells of the Δ*amiC* mutant are induced by the complete or partial lack of cell wall. In agreement with this hypothesis, the observation of viable fosfomycin-treated Δ*amiC* mutant cells was only possible when performed in the presence of 0.5 M osmoprotective sucrose, while the bacterium was uncultivable in non-osmoprotective minimal medium (data not shown).

Swollen cells of the Δ*amiC* mutant are induced in the bean bug midgut prior to a molting stage

B. insecticola symbiont cells are proliferating actively in the M4 crypts with slight fluctuations of symbiont numbers during host development due to an increase of antimicrobial activity in the M4 before molting (Kim *et al*., 2014; Ohbayashi *et al*., 2019). We analyzed spatiotemporal variations in *in vivo* cell shape of the Δ*amiC* mutant to investigate whether host physiology affects symbiont morphology during host development (Fig. 5A). The Δ*amiC* mutant was chain-forming in the whole midgut region at the early 3rd instar stage (Fig. 5B-5D), but many spherical cells were observed in the middle and posterior regions of the M4 at the middle 3rd instar stage (Fig. 5F-5G). Interestingly, most cells became spherical at all regions of the M4 at the late 3rd instar stage, immediately prior to molting (Fig. 5H-5J), and some of them were extremely swollen in the anterior and middle region of the M4 (Fig. 5H-5J). These

316 results suggested that host physiology before molting induced swollen cells in the *B.*
317 *insecticola* Δ*amiC* mutant.
318
319 **Discussion**
320 In this study, we discovered that the cell shape of the Δ*amiC* mutant of *B.*
321 *insecticola* became swollen in the midgut crypts of the bean bug (Fig. 1D), and among
322 the various *in vitro* conditions, only fosfomycin treatment could induce a similar
323 swollen shape in the Δ*amiC* mutant (Fig. 3). Moreover, the wild type also showed a
324 similar but milder phenotype (Fig. 1C-1D). These results indicate that the
325 morphological alteration observed in the *Burkholderia* symbiont in the midgut crypts
326 (Ohbayashi *et al*., 2019) is induced by a cell wall-targeting agent.
327 The *in vitro* mimicking of swollen cells by fosfomycin treatment strongly
328 suggests that the swollen shape of the Δ*amiC* mutant is due to a complete or partial lack
329 of cell wall. Indeed, the bacteria could not grow under non-osmoprotective minimal
330 medium with fosfomycin. Probably bacterial lysis occurred due to impaired cell wall
331 integrity, resulting from an inhibition of peptidoglycan precursor biosynthesis by
332 fosfomycin combined with the deletion of the *amiC* gene. In the presence of the
333 osmoprotectant sucrose, lysis was prevented in the fosfomycin-treated Δ*amiC* mutant
334 and the cells became spherical and enlarged. This morphology resembles the shape of
335 cell wall-deficient bacterial forms, called the “L-form” (Allan *et al*., 2009).
336 The “L-form” was first described in *Streptobacillus moniliformis* (“L” was named
337 in honor to the Lister Institute where the bacterial form was discovered) (Klieneberger,

338 1935). This pleomorphic bacterium is able to switch its morphology from chains to
339 swollen *in vitro* (Dienes, 1939). Subsequently, it was demonstrated that L-form bacteria
340 can be induced by suppression of the cell wall integrity with cell wall inhibiting agents
341 such as penicillin and lysozyme (Madoff, 1986). A number of studies have
342 demonstrated that L-forms can be induced in osmoprotective conditions by lytic
343 enzymes and/or inhibitors of cell wall biosynthesis, such as lysozyme, penicillin G,
344 ampicillin and fosfomycin, in diverse bacterial species including Gram-positive and
345 Gram-negative bacteria (Allan *et al*., 2009; Errington *et al*., 2016). In case of *B.*
346 *insecticola*, only fosfomycin induced L-form-like swollen cells (Fig. 3). Fosfomycin
347 targets MurA, which performs the first step in peptidoglycan synthesis (Egan *et al*.,
348 2020). However, peptidoglycan synthesis is complex, consisting of many synthesis and
349 regulatory steps (Supplementary Table S1). It is likely that other molecules inhibiting
350 steps downstream of MurA would cause similar phenotypes as fosfomycin. It remains
351 unclear why the other lytic enzymes and/or inhibitors of cell wall, including lysozyme,
352 polymyxin B, and SDS did not induce such swollen cell shape (Fig. 3). We speculate
353 that *Burkholderia* species have multiple defense mechanisms against surface-attacking
354 antimicrobial agents, which may maintain the cell shape of the Δ*amiC* mutant under
355 those membrane stress conditions. For example, modified LPS lipid A structure with a
356 positively charged 4-amino-4-deoxy-arabinose (Ara4N), membrane-integrated
357 hopanoids, and several efflux pomp mechanisms contribute to this cell envelope
358 stability (Rodes and Schweizer, 2016). C-type lysozymes, as the one used in our assays,
359 are known to hydrolyze peptidoglycan of gram-positive as well as gram-negative

bacteria. However, because in gram-negative bacteria peptidoglycan is shielded by the outer membrane, it is possible that the enzyme did not get access to the peptidoglycan substrate of *B. insecticola* in our assay. Of note, the symbiotic organ of *R. pedesteris* expresses genes encoding c-type lysozymes as well as a bacterial type of lysozyme (Futahashi *et al*., 2013). These enzymes could contribute to the modification of the cell morphology in the symbiotic organ but would require the assistance of other factors in the gut that permeabilize the outer membrane. The absence of these factors could then explain the lack of response of *B. insecticola* in our lysozyme assay. On the other hand, it is also possible that *B. insecticola* has a resistance mechanism against lysozyme activity as an adaptation to colonize the lysozyme-containing midgut crypts.

The spatiotemporal observations of the Δ*amiC* mutant in the midgut crypts revealed that symbiont cells become swollen particularly before molting (Fig. 5). Kim *et al.* (2014) reported that a temporary decrease of the symbiont population occurs before molting, when expression of genes encoding antimicrobial proteins and peptides such as c-type lysozyme and riptocin was up-regulated. In addition, these antimicrobial peptides produced in the M4 showed much stronger antimicrobial activity against *in vivo* symbiont cells than *in vitro* grown cells (Kim *et al*., 2015; Ohbayashi *et al*., 2019). Indeed, the cell envelope structure of *in vivo B. insecticola* is altered as revealed by the lack of the O-antigen polysaccharide on LPS and by the formation of blebs on the bacterial membrane (Kim *et al*., 2015; Ohbayashi *et al*., 2019). These stresses attacking the cell surface together with the deletion of the *amiC* gene probably induce the swollen cells in the M4 crypts before molting.

Although our study suggests that a peptidoglycan-targeting antimicrobial agent is secreted in the M4 crypts inducing the swollen cell shape, the nature of this agent remains unclear. In case of the legume-rhizobium symbiosis, NCR peptides in nodules block cell division in rhizobia, which induces the cell elongation in the bacteroids (Mergaert, 2020; Mergaert, 2018). In a convergent manner, a rhizobium mutant in a gene encoding a peptidoglycan-modifying DD-carboxypeptidase enzyme forms bacteroids that have a strongly enlarged and spherical shape, much like the crypt bacteria produced by the Δ*amiC* mutant described here. More specifically, this mutant forms these abnormally swollen bacteroids only in nodules that produce NCR peptides, suggesting that these peptides are the direct cause of the bacterial growth defect of the mutant (Gully et al., 2016). The bacteriocytes in the pea aphid produce bacteriocyte-specific cysteine-rich (BCR) peptides (Shigenobu and Stern, 2013). Their function *in vivo* is still unknown, but some BCR peptides showed *in vitro* antimicrobial activity, induced cell elongation, and increased membrane permeability and DNA content in *E. coli*, which is phylogenetically close to the *Buchnera* symbionts (Uchi *et al*., 2019). These BCR peptides could determine the swollen and spherical morphology of the *Buchnera* cells in the bacteriocytes. Notably, in the bean bug, over 90 species of crypt-specific cysteine-rich peptides (CCRs) are secreted in the M4 crypts (Futahashi *et al*., 2013), some of which show antimicrobial activity against *in vivo* cells of *B. insecticola* (Ohbayashi *et al*., 2019). Although there is no sequence similarity between NCR, BCR, and CCR peptides, these peptides are all small and cysteine rich, resembling typical antimicrobial peptides of innate immunity such as defensins (Futahashi *et al*., 2013;

Montiel *et al*., 2017; Mergaert *et al*., 2003; Shigenobu and Stern, 2013). This type of cysteine-rich peptides might be the result of convergent evolution in the different symbiotic systems where they could have similar functions. It would be of great interest, in future studies, to determine whether CCRs are involved in the morphological alteration of the Δ*amiC* mutant in the midgut crypts by exposing the Δ*amiC* mutant to CCR peptides *in vitro* or by analyzing the morphology of the Δ*amiC* mutant in the crypts after the suppression of CCR expression by reverse genetics in the host insect.

In conclusion, the detailed analysis of the symbiotic phenotype of the Δ*amiC* mutant enabled us to highlight the existence of a novel and partially characterized molecular mechanism of symbiont control by *R. pedestris* that might be widespread in host-microbe symbioses.

Acknowledgements

We thank Haruka Ooi (AIST-Hokkaido, Japan) for the assistance in insect maintenance, and Bok Luel Lee for kindly providing the Δ*amiC* mutant of *B. insecticola*. This study is supported by Japan Society for the Promotion of Science (JSPS) Research Fellowships for Young Scientists to TO (grant numbers 20170276 and 19J01106), the JSPS KAKENHI to YK (20H03303), and the JSPS-CNRS Bilateral Open Partnership Joint Research Project to YK and PM.

References

Allan, E.J., Hoischen, C., and Gumpert, J. (2009) Bacterial L- Forms. *Adv Appl Microbiol* **68**: 1-39.

Baumann P. (2005) Biology of bacteriocyte-associated endosymbionts of plant sap-sucking insects. *Annu Rev Microbiol* **59**: 155-189.

Bublitz, D.C., Chadwick, G.L., Magyar, J.S., Sandoz, K.M., Brooks, D.M., Mesnage, S., *et al*. (2019) Peptidoglycan production by an insect-bacterial mosaic. *Cell* **179**: 703-712.

Czernic, P., Gully, D., Cartieaux, F., Moulin, L., Guefrachi, I., Patrel, D., *et al*. (2015) Convergent evolution of endosymbiont differentiation in dalbergioid and inverted repeat-lacking clade legumes mediated by nodule-specific cysteine-rich peptides. *Plant Physiol* **169**: 1254-1265.

Dienes, L. (1939) L organisms of Klieneberger and *Streptobacillus moniliformis*. *J infect Dis* **65**: 24-42.

Egan, A.J.F., Errington, J., and Vollmer, W. (2020) Regulation of peptidoglycan synthesis and remodelling. *Nat Rev Microbiol* https://doi.org/10.1038/s41579-020-0366-3 (Epub ahead of print).

Errington, J., Mickiewicz, K., Kawai, Y., and Wu L.J. (2016) L-form bacteria, chronic diseases and the origins of life. *Philos Trans R Soc Lond B Biol Sci* **371**: 20150494.

Falagas, M.E., Vouloumanou, E.K., Samonis, G., and Vardakas, K.Z. (2016) Fosfomycin. *Clin Microbiol Rev* **29**: 321-347.

Futahashi, R., Tanaka, K., Tanahashi, M., Nikoh, N., Kikuchi, Y., Lee, B.L., *et al*. (2013) Gene expression in gut symbiotic organ of stinkbug affected by extracellular bacterial symbiont. *PLoS One* **8**: e64557.

Gully, D., Gargani, D., Bonaldi, K., Grangeteau, C., Chaintreuil, C., Fardoux, J., *et al*. (2016) A peptidoglycan-remodeling enzyme is critical for bacteroid

differentiation in *Bradyrhizobium* spp. during legume symbiosis. *Mol Plant Microbe Interact* **29**: 447-457.

Heidrich, C., Templin, M.F., Ursinus, A., Merdanovic, M., Berger, J., Schwarz, H., *et al.* (2001) Involvement of N-acetylmuramyl-L-alanine amidases in cell separation and antibiotic-induced autolysis of *Escherichia coli*. *Mol Microbiol* **41**: 167-178.

Hirota, B., Okude, G., Anbutsu, H., Futahashi, R., Moriyama, M., Meng, X.Y., *et al.* (2017) A novel, extremely elongated, and endocellular bacterial symbiont supports cuticle formation of a grain pest beetle. *Mbio* **8**: e01482-17.

Itoh, H., Jang, S., Takeshita, K., Ohbayashi, T., Ohnishi, N., Meng, X.Y., *et al.* (2019) Host-symbiont specificity determined by microbe-microbe competition in an insect gut. *Proc Natl Acad Sci U S A* **116**: 22673-22682.

Kaltenpoth, M., and Flórez, L.V. (2020) Versatile and dynamic symbioses between insects and *Burkholderia* bacteria. *Annu Rev Entomol* **65**: 145-170.

Kawai, Y., Mercier, R., Wu, L.J., Dominguez-Cuevas P., Oshima T., and Errington J. (2015) Cell growth of wall-free L-form bacteria is limited by oxidative damage. *Curr Biol* **25**: 1613-1618.

Kikuchi, Y., and Fukatsu, T. (2014) Live imaging of symbiosis: spatiotemporal infection dynamics of a GFP-labelled *Burkholderia* symbiont in the bean bug *Riptortus pedestris*. *Mol Ecol* **23**: 1445-1456.

Kikuchi, Y., Hosokawa, T., and Fukatsu, T. (2007) Insect-microbe mutualism without vertical transmission: a stinkbug acquires a beneficial gut symbiont from the environment every generation. *Appl Environ Microbiol* **73**: 4308-4316.

Kikuchi, Y., Hosokawa, T., and Fukatsu, T. (2011) Specific developmental window for establishment of an insect-microbe gut symbiosis. *Appl Environ Microbiol* **77**: 4075-4081.

Kim, J.K., Han, S.H., Kim, C.H., Jo, Y.H., Futahashi, R., Kikuchi, Y., *et al*. (2014) Molting-associated suppression of symbiont population and up-regulation of antimicrobial activity in the midgut symbiotic organ of the *Riptortus-Burkholderia* symbiosis. *Dev Comp Immunol* **43**: 10-14.

Kim, J.K., Son, D.W., Kim, C.H., Cho, J.H., Marchetti, R., Silipo, A., *et al*. (2015) Insect gut symbiont susceptibility to host antimicrobial peptides caused by alteration of the bacterial cell envelope. *J Biol Chem* **290**: 21042-21053.

Klieneberger, E. (1935) The natural occurrence of pleuropneumonia-like organisms in apparent symbiosis with *Streptobacillus moniliformis* and other bacteria. *J Pathol Bacteriol* **40**: 93-105.

Lee, J.B., Byeon, J.H., Jang, H.A., Kim, J.K., Yoo, J.W., Kikuchi Y., *et al*. (2015) Bacterial cell motility of *Burkholderia* gut symbiont is required to colonize the insect gut. *FEBS Lett* **589**: 2784-2790.

Login, F.H., Balmand, S., Vallier, A., Vincent-Monegat, C., Vigneron, A., Weiss-Gayet, M., *et al*. (2011) Antimicrobial peptides keep insect endosymbionts under control. *Science* **334**: 362-365.

Lukasik, P., Newton, J.A., Sanders, J.G., Hu, Y., Moreau, C.S., Kronauer, D.J.C., *et al*. (2017) The structured diversity of specialized gut symbionts of the new world army ants. *Mol Ecol*. **26**: 3808-3825.

Madoff, S. (1986). The Bacterial L-Forms. Marcel Decker, New York.

Mergaert, P. (2020) Differentiation of symbiotic nodule cells and their rhizobium endosymbionts. *Adv Bot Res* **94**: 149-180.

Mergaert, P. (2018) Role of antimicrobial peptides in controlling symbiotic bacterial populations. *Nat Prod Rep* **35**: 336-356.

Mergaert, P., Nikovics, K., Kelemen, Z., Maunoury, N., Vaubert, D., Kondorosi, A., *et al*. (2003) A novel family in *Medicago truncatula* consisting of more than 300 nodule-specific genes coding for small, secreted polypeptides with conserved cysteine motifs. *Plant Physiol* **132**: 161-173.

505 Mergaert, P., Uchiumi, T., Alunni, B., Evanno, G., Cheron, A., Catrice, O., *et al*. (2006)
506 Eukaryotic control on bacterial cell cycle and differentiation in the *Rhizobium*-
507 legume symbiosis. *Proc Natl Acad Sci U S A* **103**: 5230-5235.
508 Montiel, J., Downie, J.A., Farkas, A., Bihari, P., Herczeg, R., Balint, B., *et al*. (2017)
509 Morphotype of bacteroids in different legumes correlates with the number and
510 type of symbiotic NCR peptides. *Proc Natl Acad Sci U S A* **114**: 5041-5046.
511 Okude, G., Koga, R., Hayashi, T., Nishide, Y., Meng, X.Y., Nikoh, N., *et al*. (2017)
512 Novel bacteriocyte-associated pleomorphic symbiont of the grain pest beetle
513 *Rhyzopertha dominica* (Coleoptera: Bostrichidae). *Zoological Lett* **3**: 13.
514 Ohbayashi, T., Futahashi, R., Terashima, M., Barriere, Q., Lamouche, F., Takeshita, K.,
515 *et al*. (2019) Comparative cytology, physiology and transcriptomics of
516 *Burkholderia insecticola* in symbiosis with the bean bug *Riptortus pedestris* and
517 in culture. *ISME J* **13**: 1469–1483.
518 Ohbayashi, T., Mergaert, P., and Kikuchi, Y. (2020) Host-symbiont specificity in
519 insects: Underpinning mechanisms and evolution. *Adv Insect Physiol* **58**: 27-62.
520 Ohbayashi, T., Takeshita, K., Kitagawa, W., Nikoh, N., Koga, R., Meng, X.Y., *et al*.
521 (2015) Insect's intestinal organ for symbiont sorting. *Proc Natl Acad Sci U S A*
522 **112**: E5179–E5188.
523 Oke, V., and Long, S.R. (1999) Bacteroid formation in the *Rhizobium*-legume
524 symbiosis. *Curr Opin Microbiol* **2**: 641-646.
525 Rhodes, K.A., and Schweizer, H.P. (2016) Antibiotic resistance in *Burkholderia*
526 species. *Drug Resist Updat* **28**:82-90.
527 Schmidtke, L.M., and Carson, J. (1999) Induction, characterisation and pathogenicity in
528 rainbow trout *Oncorhynchus mykiss* (Waldbaum) of *Lactococcus gravieae* L-
529 forms. *Vet Microbiol Immunol* **69**: 287-300.
530 Schneider C.A., Rasband W.S., and Eliceiri K.W. (2012) NIH Image to ImageJ: 25
531 years of image analysis. *Nature Methods*. **9**: 671-5.

Shigenobu S., and Stern D.L. (2013) Aphids evolved novel secreted proteins for symbiosis with bacterial endosymbiont. *Philos Trans R Soc Lond B Biol Sci* **280**: 20121952.

Shigenobu, S., and Wilson A.C. (2011) Genomic revelations of a mutualism: the pea aphid and its obligate bacterial symbiont. *Cell Mol Life Sci* **68**: 1297-1309.

Strang J.A., Allan, E. J., Seddon, B., and Paton, A. M. (1991) Induction of *Bacillus brevis* L-forms. *J Appl Bacteriol* **70**: 47-51.

Takeshita, K., and Kikuchi, Y. (2017) *Riptortus pedestris* and *Burkholderia* symbiont: an ideal model system for insect-microbe symbiotic associations. *Res Microbiol* **168**: 175-187.

Uchi, N., Fukudome, M., Nozaki, N., Suzuki, M., Osuki, K.I., and Shigenobu, S., *et al*. (2019) Antimicrobial activities of cysteine-rich peptides specific to bacteriocytes of the pea aphid *Acyrthosiphon pisum*. *Microbes Environ* **34**: 155-160.

van Teeseling, M.C.F., de Pedro, M.A., and Cava, F. (2017) Determinants of bacterial morphology: from fundamentals to possibilities for antimicrobial targeting. *Front Microbiol* **8**:1264.

Young, K.D. (2006) The selective value of bacterial shape. *Microbiol Mol Biol Rev* **70**: 660-703.

Figure legends

Fig. 1. *In vitro* and *in vivo* cell morphology in *B. insecticola* wild-type strain RPE225 and the Δ*amiC* mutant

Epifluorescence microscopy photos of (A, B) *in vitro* (cultured in YG medium) and (C, D) *in vivo* (colonizing the M4 at a 3rd instar nymph) bacterial cells in (A, C) the wild-type strain RPE225 and in (B, D) the Δ*amiC* mutant. Arrowheads indicate (C) spherical cells and (D) swollen cells. Quantitative analysis of each cell sample is shown in Fig. 2. Scale bars: 5 μm.

Fig. 2. Relative abundance of cellular morphology in *in vitro* and *in vivo B. insecticola* wild type and Δ*amiC* mutant

Relative abundance of cellular morphology by (A-D) aspect ratio distribution and by (E-H) major axis and minor axis lengths distribution in *in vitro* grown (A, E) wild type and (B, F) Δ*amiC* mutant, and *in vivo* (C, G) wild type and (D, H) Δ*amiC* mutant. The color indicates bacterial cell morphology. Orange indicates elongated cells with aspect ratio less than 0.3, green indicates rod-shaped cells with aspect ratio between 0.3 and 0.8, and blue indicates spherical cells with aspect ratio between 0.8 and 1.0. The number of investigated cells in each condition is shown in each figure.

Fig. 3. *In vitro* induction of swollen cells in *B. insecticola* wild type and Δ*amiC* mutant

573 Epifluorescence microscopy images of the wild type and the Δ*amiC* mutant cells
574 cultured in (A) different carbon sources, and after exposure to (B) stresses against the
575 cell membrane or (C) osmotic stresses. Quantitative analysis of each cell sample is
576 shown in Fig. 4 and Supplementary Fig. S3. Scale bars: 5 μm.
577
578 **Fig. 4. Distribution of cellular morphology in *B. insecticola* wild type and Δ*amiC***
579 **mutant after fosfomycin exposure**
580 Cellular morphology determined by (A-D) aspect ratio distribution and by (E-H) major
581 axis and minor axis lengths distribution in (A, B, E, F) an osmoprotective MMMSM
582 medium and (C, D, G, H) after fosfomycin exposure in MMMSM medium in (A, C, E,
583 G) the wild type and (B, D, F, H) the Δ*amiC* mutant. The color code indicates bacterial
584 cell morphology as in Fig. 2. The number of investigated cells in each condition is
585 shown in each figure.
586
587 **Fig. 5. Cell morphology of the Δ*amiC* mutant colonizing the M4 crypts**
588 (A) The whole region of M4 crypts of a 3rd instar nymph of *R. pedestris*. Scale bar: 0.5
589 mm. (B-J) The Δ*amiC* mutant colonizing the M4 crypts (B-D) at 3rd instar early stage,
590 (E-G) at 3rd instar middle stage and (H-J) at 3rd instar late stage. (B, E, H) The anterior
591 region, (C, F, I) middle region and (D, G, J) posterior region of the M4 are shown.
592 Green and blue signals indicate symbiont-derived GFP and host nuclear DNA,
593 respectively. Scale bars: 10 μm.
594

Fig. 1

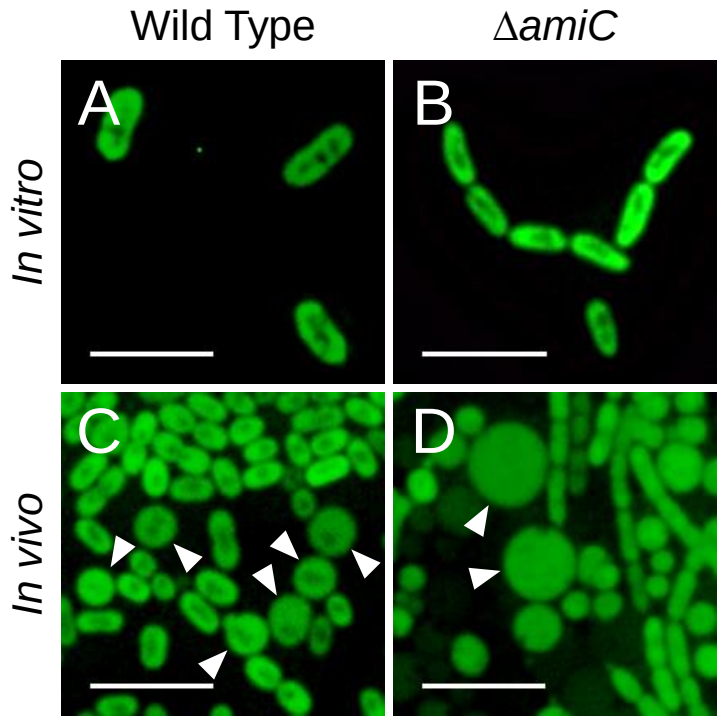

Fig. 2

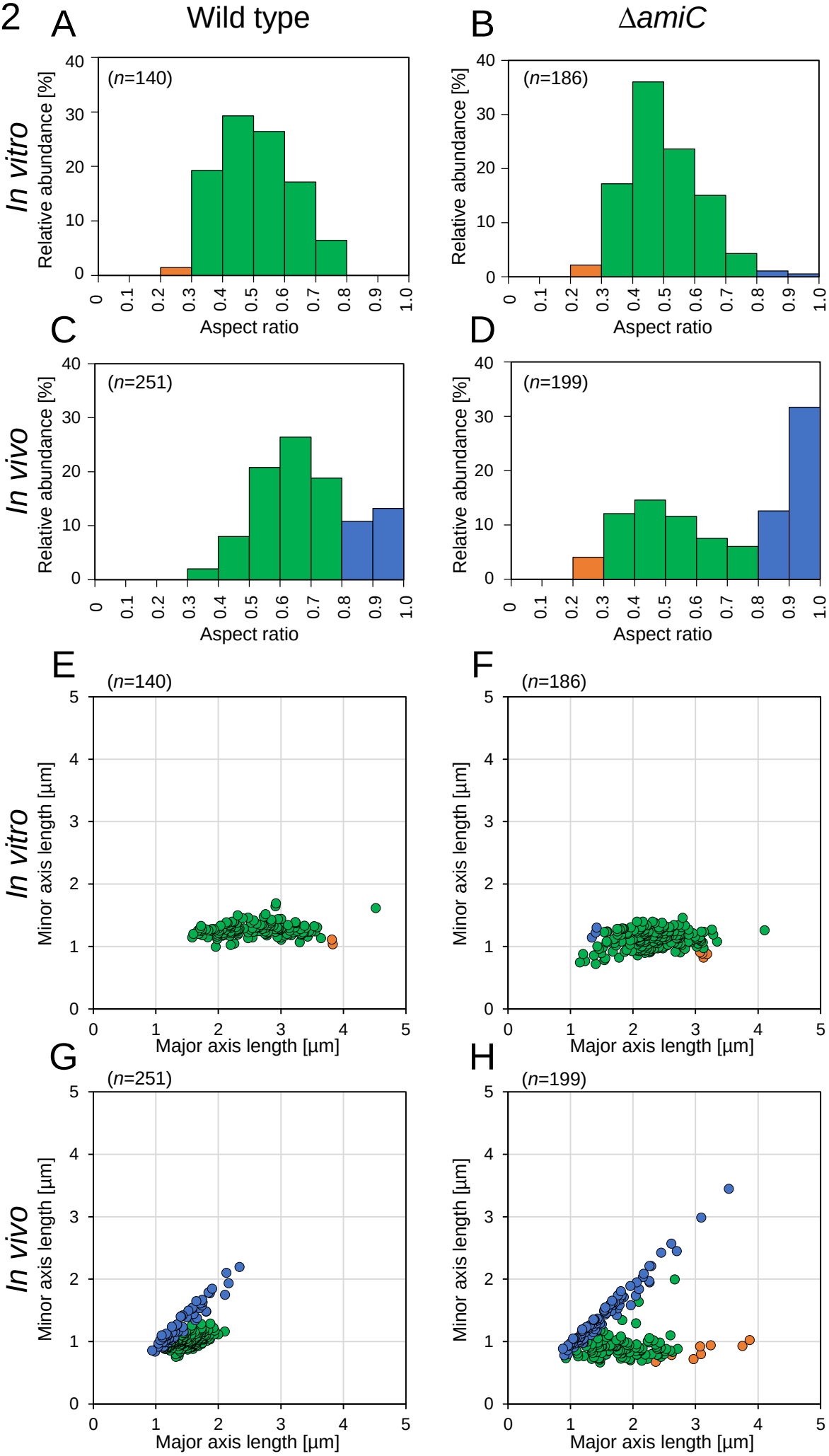
A
Wild type
B
ΔamiC
In vitro
In vivo
Relative abundance [%]
(n=140)
(n=186)
(n=251)
(n=199)
Aspect ratio
C
D
E
F
G
H
Minor axis length [µm]
Major axis length [µm]

Fig. 3

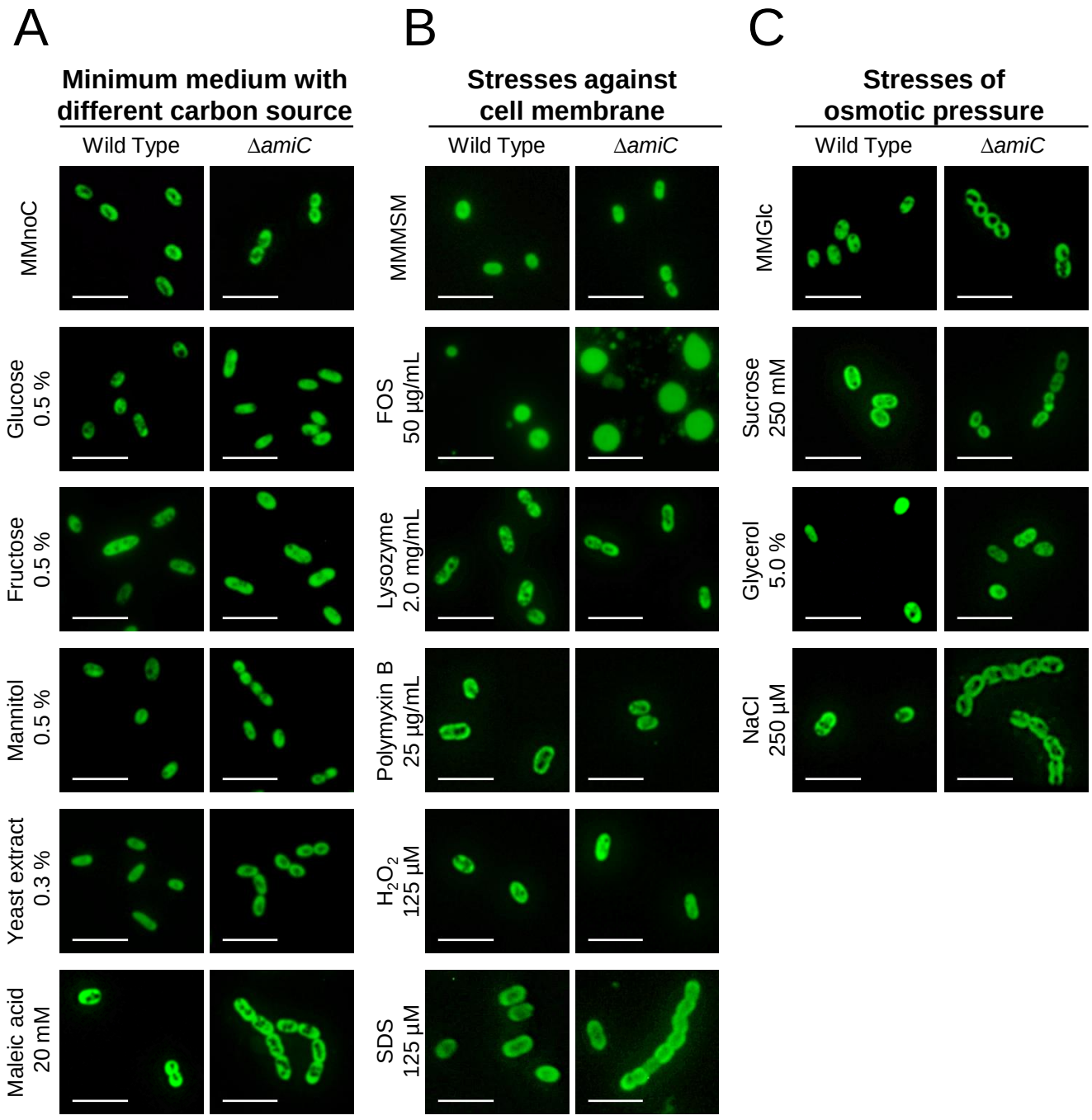
A
Minimum medium with different carbon source
Wild Type
ΔamiC
MMnoC
Glucose 0.5 %
Fructose 0.5 %
Mannitol 0.5 %
Yeast extract 0.3 %
Maleic acid 20 mM
B
Stresses against cell membrane
Wild Type
ΔamiC
MMMSM
FOS 50 µg/mL
Lysozyme 2.0 mg/mL
Polymyxin B 25 µg/mL
H2O2 125 µM
SDS 125 µM
C
Stresses of osmotic pressure
Wild Type
ΔamiC
MMGlc
Sucrose 250 mM
Glycerol 5.0 %
NaCl 250 µM

Fig. 4

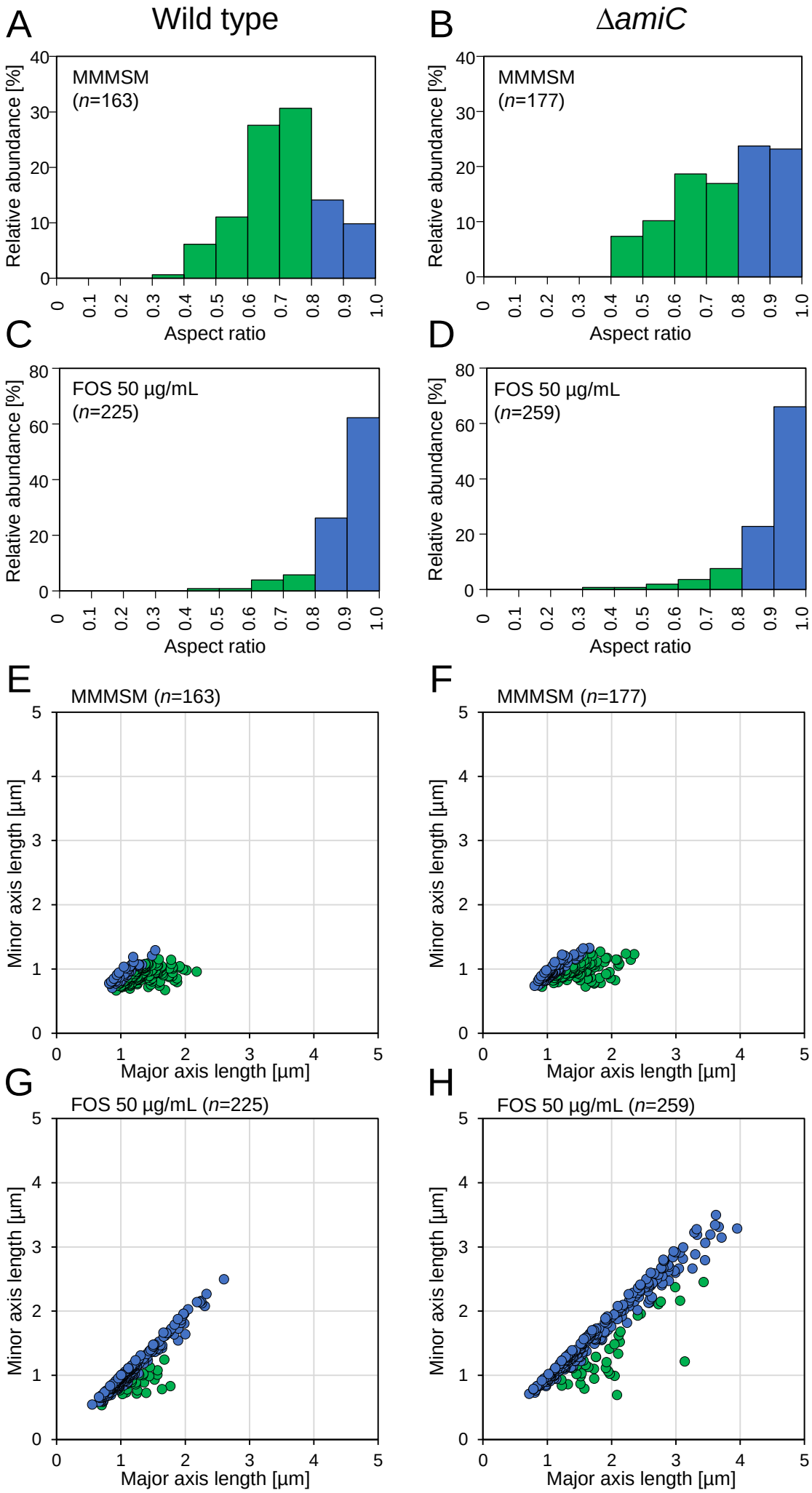
A
Wild type
B
ΔamiC
MMMSM
(n=163)
MMMSM
(n=177)
Relative abundance [%]
Aspect ratio
C
D
FOS 50 µg/mL
(n=225)
FOS 50 µg/mL
(n=259)
E
F
MMMSM (n=163)
MMMSM (n=177)
Minor axis length [µm]
Major axis length [µm]
G
H
FOS 50 µg/mL (n=225)
FOS 50 µg/mL (n=259)

Fig. 5

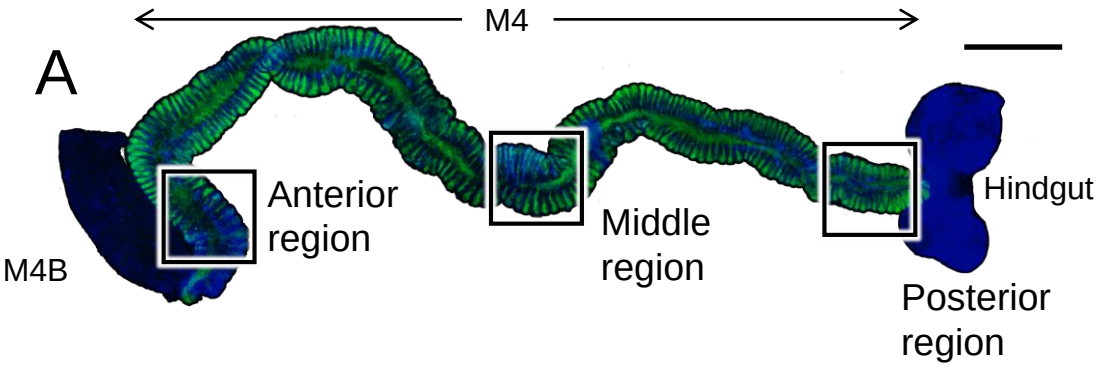
A
M4
M4B
Anterior region
Middle region
Posterior region
Hindgut

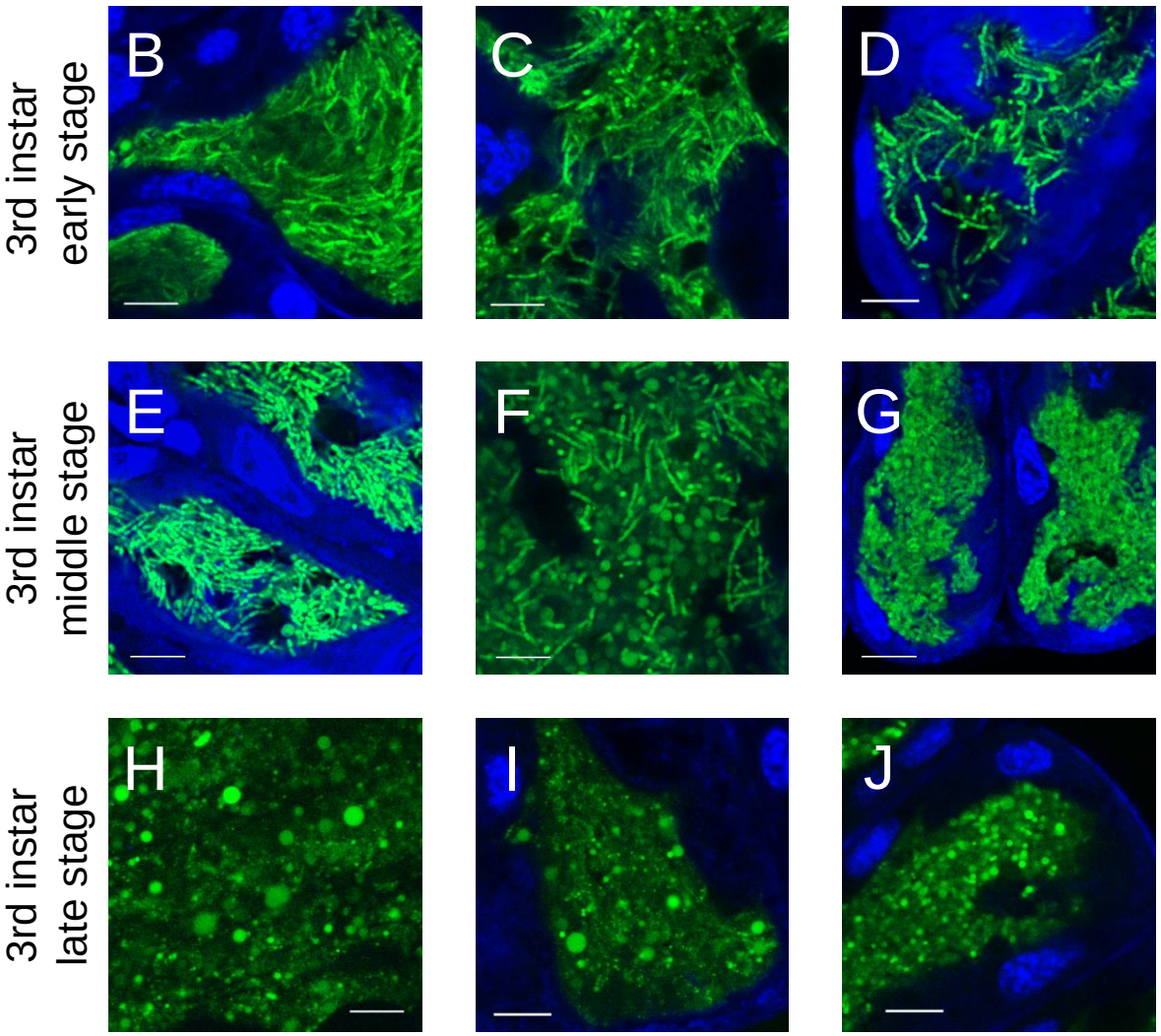
3rd instar early stage
3rd instar middle stage
3rd instar late stage
B
C
D
E
F
G
H
I
J